Journal of Electronic Imaging 6(4), 426–438 (October 1997).

Generalized support constraint for three-dimensional reconstruction from incomplete Fourier spectra

Etienne Payot
CEA-LETI/DSYS
17, avenue des Martyrs
38054 Grenoble Cedex 9, France
E-mail: payot@dsys.ceng.cea.fr

Françoise J. Prêteux
Institut National des Télécommunications
9, rue Charles Fourier
91011 Evry Cedex, France

Yves Trousset
G. E. Medical Systems
283, rue de la Miniere
78533 Buc Cedex, France

Régis Guillemaud
CEA-LETI/DSYS
17, avenue des Martyrs
38054 Grenoble Cedex 9, France

Abstract. *Many imaging systems involve a loss of information that requires the incorporation of prior knowledge in the restoration/reconstruction process. We focus on the typical case of 3D reconstruction from an incomplete set of projections. An approach based on constrained optimization is introduced. This approach provides a powerful mathematical framework for selecting a specific solution from the set of feasible solutions; this is done by minimizing some criteria depending on prior densitometric information that can be interpreted through a generalized support constraint. We propose a global optimization scheme using a deterministic relaxation algorithm based on Bregman's algorithm associated with half-quadratic minimization techniques. When used for 3D vascular reconstruction from 2D digital subtracted angiography (DSA) data, such an approach enables the reconstruction of a well-contrasted 3D vascular network in comparison with results obtained using standard algorithms.* © *1997 SPIE and IS&T.* [S1017-9909(97)00404-2]

1 Introduction

In many computer imaging applications, such as medical, astronomical, or geophysical imaging, the measured data result from the transformation of an unknown physical parameter. The recovery of the physical parameter from the measured data, called the inverse problem, is ill-posed since Hadamard's conditions are not satisfied, more precisely:

1. The existence of a solution is not mathematically guaranteed.
2. The solution, when it exists, is unstable with respect to the noise due to the noncontinuity of the inverse mapping. In the discrete case, this noncontinuity results in an ill-conditioned inverse matrix.
3. The solution may be nonunique. This situation arises when dealing with an incomplete measured data set, which leads to a nonbiunivoque transformation between the observed data and the map of the physical parameter to be reconstructed. The lack of data results in the existence in the Hilbert space of a null space about which the available data do not provide any information. In this case, corresponding discrete operators are singulars.

In this paper, we exclusively address the nonuniqueness problem resulting from an incomplete data set. This problem is a key problem in many computerized tomographic (CT) applications whenever projection data are limited in number and possibly in range of the viewing angle.

We are interested in the specific application of 3D vas-

Paper IST-04 received Jan. 9, 1997; revised manuscript received May 27, 1997; accepted for publication May 29, 1997. This paper is a revision of a paper presented at the SPIE conference on Statistical and Stochastic Methods for Image Processing, Aug. 1996, Denver, CO. The paper presented there appears (unrefereed) in SPIE Proceedings Vol. 2823.
1017-9909/97/$10.00 © 1997 SPIE and IS&T.

cular reconstruction. The principle consists of recovering the 3D image of a blood vessel network from a set of 2D digital subtracted angiography (DSA) data acquired during a rotation around the patient. In DSA, x-ray projections are acquired before and during injection of a contrast agent into the vessels. Subtracting both images enhances the visibility of vessels by removing bony structures. The short time of stability of the contrast agent does not allow the acquisition of a large number of projections. In addition, a circular acquisition trajectory of the imaging system does not fulfill the data completeness requirement for 3D reconstruction.[1]

In this paper, the problem of an incomplete data set in 3D vascular reconstruction is addressed by introducing densitometric prior information. This information is used in a functional to be minimized. In Section 2, the problem of the nonuniqueness is mathematically addressed in detail and is reformulated as missing data in the Fourier domain. In Section 3, the constrained optimization framework is introduced for selecting an element from the null space by minimizing a specific functional. Bregman's minimization algorithm is described in detail and its limitations are discussed. In Section 4, the method and the algorithm that we propose are developed. A deterministic relaxation algorithm based on half-quadratic minimization is proposed for handling a wide class of criteria to be minimized. In Section 5, the efficiency of the algorithm is discussed using synthetic and real data.

2 Problem of Nonuniqueness

A 3D discrete image of size n is represented by a real-valued function x defined on some domain Ω. This domain is partitioned into a finite number of volume elements (voxels) labeled in an arbitrary way from 1 to n. Assuming that x is constant within each voxel, function x can be expressed as $x=\Sigma_{j=1}^{n} x_j \mathbb{I}_j$, where $\mathbb{I}_j$ denotes the indicator function of the j'th voxel and x is represented by the vector $[x_1,\ldots,x_n]^T$. In x-ray tomography, x corresponds to the attenuation coefficient to be recovered from the available data consisting of line or strip integrals along each ray path. These latter measured values are denoted by $y=[y_1,\ldots,y_m]^T$, where m denotes the number of acquired integral rays.

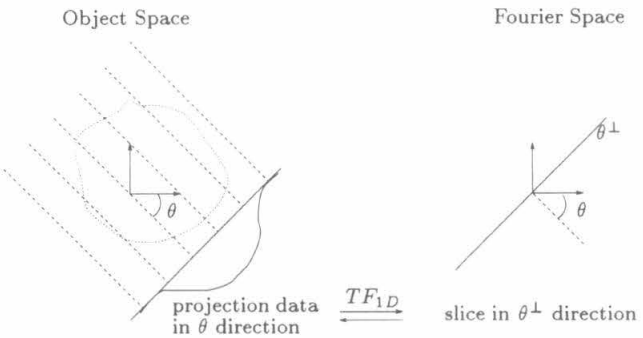

Fig. 1 Projection theorem (TF_{1D} stands for the 1D Fourier transform).

Within this framework, the CT problem can be stated as follows: given a set of measurements y_i $\{i=1,\ldots,m\}$, recover the "best" estimate $\bar{x}$ of the attenuation function x.

The feasible set is identified with the set of vectors satisfying the image formation equations:

$$\mathbf{H}x=y, \tag{1}$$

where $\mathbf{H}$ is the $n\times m$ projection matrix whose i'th row is formed by H_i.

When the projections are limited in number or in angular range, the projection operator $\mathbf{H}$ becomes singular, and its associated null space, $\ker\{\mathbf{H}\}$, defined by the eigenvectors associated to null eigenvalues, is not reduced to the null vector. In other words, this means that nonzero vectors x exist whose projections are null.

This situation is well illustrated using the projection or Fourier slice theorem (Fig. 1), which states that the Fourier transform of the projection data in the direction θ equals the slice of Fourier transform of the object in the direction orthogonal to θ. Thus, projection data that are restricted in angular range or in number lead to missing sectors in the Fourier transform of the image (Fig. 2).

If the missing sectors are not filled, deformation of large objects, intensity underestimation of high frequency objects and undersampling artifacts will result from inverse transformations. Klug and Crowther[2] showed that a complete

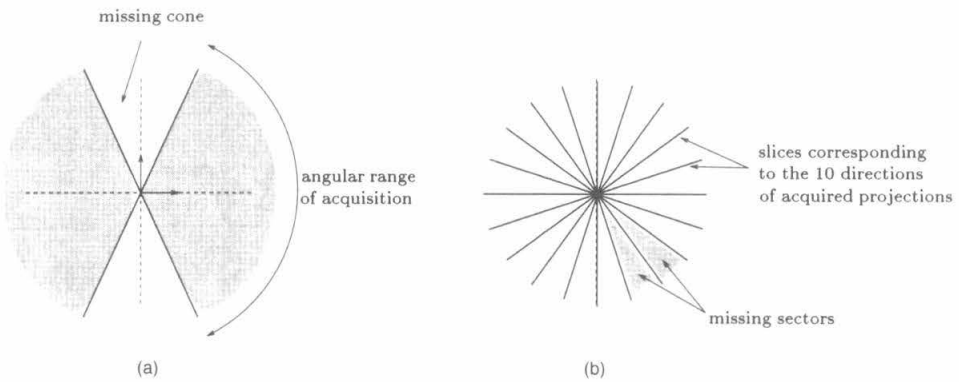

Fig. 2 Typical representation of an incomplete data set in the Fourier domain for a limited angular range (a) and for a reduced number of projections with a regular and sparse angular sampling (b).

data set (i.e., satisfying Shannon's sampling constraint) requires $(\pi/2)N$ projections equally distributed over 180 deg for a reconstruction of size N^3. He observed practically that this constraint can be relaxed to N directions without leading to striking undersampling artifacts. In vascular imaging, such a condition cannot be satisfied; the vessels have a small size (typically from 1 to 10 voxels of diameter) and require high reconstruction resolution (typically 512^3) whereas the number of projections is limited to a few tens due to the specific acquisition procedure.

One key aspect in 3D reconstruction from incomplete data consists of selecting a "suitable" element of ker{**H**} (i.e., a component on the missing Fourier domain), possibly depending on prior information.

Standard inversion methods, which provide the minimal norm solution or generalized inverse solution, cannot take into account a missing sector component since this specific solution possesses a zero null-space component. Hence, the recovery of such a component requires spectrum extrapolation techniques.

Spectrum extrapolation was first addressed by Gerchberg[3] by using the Paley-Wiener theorem, which claims that the Fourier transform of an object is uniquely determined by its values on a compact domain Ω of the Fourier space. Assuming that the unknown function x vanishes outside some known bounded domain denoted by $\mathrm{supp}(x)$. Gerchberg[3] and Papoulis[4] proposed an iterative back and forth algorithm between object and frequency space to analytically extend the known spectrum onto the missing domain. Let us denote by $\mathbb{I}_{\mathrm{supp}(x)}$ the domain indicator in the object space, $\mathbb{I}_{\bar{\Omega}}$ the operator that sets to zero the known domain Ω in the Fourier space and $\hat{x}_0$ the known Fourier spectrum on Ω. Then Gerchberg-Papoulis's algorithm can be expressed in the Fourier space by the iterative equation:

$$\hat{x}_{n+1} = \hat{x}_0 + \mathbb{I}_{\bar{\Omega}} \cdot \mathrm{TF} \cdot \mathbb{I}_{\mathrm{supp}(x)} \cdot \mathrm{TF}^{-1} \hat{x}_n , \tag{2}$$

where TF stands for the Fourier transform. This equation can also be written in a convolution form, which provides a clear understanding of the extrapolation mechanism:

$$\hat{x}_{n+1} = \mathrm{sinc}_{\mathrm{supp}} * (\hat{x}_0 + \mathbb{I}_{\bar{\Omega}} \cdot \hat{x}_n). \tag{3}$$

This equation shows that the extrapolation in the Fourier domain results from the successive convolution of spectrum of the current estimate by the Fourier transform of the support constraint $\mathrm{sinc}_{\mathrm{supp}}$. This approach has been adapted to 2D reconstruction from projections,[5,6] but it is of limited interest in many imaging procedures since it requires the knowledge of the support of the object to be reconstructed. Moreover, even if the exact support constraint is known, this procedure cannot provide a significant extrapolation in such a case as vascular reconstruction. Indeed, the 3D vascular image is composed of a sparse, highly contrasted structure (the vascular network) surrounded by a low density wide background corresponding to the opacification of microvessels. This background makes it necessary to use too large a support (in comparison to the vascular network) to provide a significant extrapolation. This limitation can be well understood through Equation (3) in which the convolution/extrapolation kernel $\mathrm{sinc}_{\mathrm{supp}}$ reduces to a Dirac-like kernel when using such a wide support. On the other hand, neglecting the background by using a support smaller than the background results in high density pointwise artifacts due to local concentration of the density that cannot be replaced in its true position (i.e., outside of the imposed support).

Another way to handle incomplete data was investigated by using a maximum-entropy method which, quoting Jaynes,[7] selects in the feasible set the "maximally noncommittal solution with regards to missing information." In CT imaging, two popular algorithms provide such a solution: MART and MENT. MART (multiplicative algebraic reconstruction techniques) was initially proposed by Herman et al.[8] and its convergence property was established by Lent.[9] MENT (maximum entropy[10] performs the optimization scheme in the dual space in the sense of the Lagrangian formalism. These two algorithms have been extensively used for reconstruction from a few projections and have demonstrated their effectiveness.[11]

In the following, we focus on the constrained optimization techniques, which we show to be closely related to the notion of support.

3 Constrained Optimization Methods

3.1 *Optimization Framework: Lagrangian Formalism*

The optimization problem can be mathematically stated as follows:

$$\begin{cases} \min F(x) \\ x \\ \text{subject to (s.t.) } Hx = y, \end{cases} \tag{4}$$

where F is the criterion to be minimized for selecting a specific element in the feasible set of solutions.

For the optimal solution, the Lagrangian operator:

$$L(x,\lambda) = F(x) + \lambda^T (Hx - y), \tag{5}$$

should be minimal ($\lambda \in \mathbb{R}^n$ denotes the Lagrangian parameter). Hence, each first partial derivative of L should equal zero, leading to:

$$\begin{cases} \dfrac{\partial L}{\partial \lambda} \\ \dfrac{\partial L}{\partial x} \end{cases} \Rightarrow \begin{cases} Hx = y \\ \nabla F(x) = -H^T \lambda. \end{cases} \tag{6}$$

The equation $Hx = y$ corresponds to the image formation model, whereas $\nabla F(x) = -H^T \lambda$ expresses that the gradient of the criterion should belong to the range space of $\mathbf{H}^T$. This means that, considering the optimal solution $\bar{x}$, the component of $\nabla F(\bar{x})$ on the null space is zero. Indeed, if $\nabla F(\bar{x})$ has a nonzero null-space component, it is possible to find a solution that satisfies $Hx = y$ with a lower value of the criterion.

This property, which shows the advantage of the constrained optimization approach, is directly exploited in the row-action algorithm proposed by Bregman.[12]

3.2 *Bregman's Algorithm*

Let S be a nonempty, open and convex set such that its topological closure $\bar{S}$, is included in $\mathbb{R}$ ($\bar{S} \subseteq \mathbb{R}$). Let us assume that the criterion F satisfies the following conditions:

- Criterion F has continuous first partial derivatives at any point $x \in S$.
- Criterion F is a strictly convex function on $\bar{S}$.
- Criterion F is a continuous function on $\bar{S}$.

Starting from F, Bregman derived the function D of two variables (x,z) from $\bar{S} \times S$ into $\mathbb{R}$ as follows:

$$D(x,z) = F(x) - F(z) - \langle \nabla F(z), x - z \rangle, \tag{7}$$

where $\langle .,. \rangle$ stands for the usual inner product in the n-dimensional Euclidean space $\mathbb{R}^n$. Then, the D-projection x^* of a point x onto a set Ω is uniquely defined by:

$$D(x^*,x) = \min_{z \in \Omega \cap S} D(z,x). \tag{8}$$

If Ω denotes the hyperplane defined by $\langle H_i, x \rangle = y_i$, then Equation (8) becomes:

$$\nabla F(x^*) = \nabla F(x) + H_i^T \lambda, \tag{9}$$

where λ being the unique real number such that:

$$\langle H_i, x^* \rangle = y_i .$$

Equation (9) explicitly uses the property that the gradient of the criterion belongs to the range-space of $\mathbf{H}^T$.

To find the solution of the global optimization problem, Bregman proposed an iterative algorithm that performs the successive D-projections onto the hyperplane associated with each row of $\mathbf{H}$:

initialization: $x^0 \in S \cap R\{\mathbf{H}^T\}$

($R\{\mathbf{H}^T\}$ stands for the range-space of $\mathbf{H}^T$),

iterative step: $\nabla F(x^{k+1}) = \nabla F(x^k) + H_{i_k}^T \lambda$

with λ such that $\langle H_{i_k}, x^{k+1} \rangle = y_{i_k}$, (10)

cyclic control sequence: $i_k = k[\mathrm{mod}(m)] + 1$

where m is the row number of $\mathbf{H}$.

Bregman showed that the sequence of approximation $\{x^k\}$ converges toward the unique solution of Equation (4), provided that F satisfies the conditions previously mentioned.

Using the Bregman's algorithm, two specific expressions of the criterion F are of a great interest. The first case corresponds to the norm projection and is associated with $F(x) = 1/2\|x\|^2$ and $S = \mathbb{R}^n$. The D-projection operator corresponds to the orthogonal projection. In this case, Bregman's algorithm recovers the standard ART (algebraic reconstruction technique) algorithm,[8] which is known to converge to the minimal norm solution provided that x^0 belongs to the range space of $\mathbf{H}^T$. Under these conditions, Equation (10) yields the following iterative equation:

initialization: $x^0 = 0$,

iterative step: $x^{k+1} = x^k + H_{i_k}^T \left(\dfrac{y_{i_k} - \langle H_{i_k}, x^k \rangle}{H_{i_k} H_{i_k}^T} \right)$.

The second case is associated with $F(x) = \sum_{j=1}^{m} x_j \ln x_j$ and $S = \mathbb{R}^{+n}$. The associated D-projection can be interpreted as an entropic projection leading to the following iterative scheme:

initialization: $x^0 = e^{-1}$

iterative step: $\begin{cases} x^{k+1} = x^k \exp(H_{i_k}^T \lambda) \\ \lambda \text{ such that } \langle H_{i_k}, x^{k+1} \rangle = y_{i_k}. \end{cases}$

Under the very specific assumption that all the elements of $\mathbf{H}$ equal 0 or 1, the iterative equation can be written:

$$x^{k+1} = x^k \left(\frac{y_{i_k}}{\langle H_{i_k}, x^k \rangle} \right).$$

This iterative scheme is equivalent in this specific case of a MART algorithm given by[9]

$$x^{k+1} = x^k \left(\frac{y_{i_k}}{\langle H_{i_k}, x^k \rangle} \right)^{h_{i_k}}.$$

The assumpton of $\mathbf{H}$ being composed only by 0 or 1 elements corresponds to an oversimple projection formation model in which $h_{ij} = 1$ if the i'th ray intersects the j'th voxel and $h_{ij} = 0$ otherwise.

Bregman's algorithm presents several advantages:

- For some particular expression of the criteria F, this algorithm has a form similar to standard tomographic algorithms such as ART or MART.
- Row-action algorithms have demonstrated their effectiveness for handling huge and sparse matrices and for their convergence rate. Although the final convergence generally requires an infinite number of iterations, an acceptable approximation can usually be found for finite (and rather small) values of k.
- It is formulated for an arbitrary expression of the criteria provided that the function F is strictly convex and continuously differentiable.

Nevertheless, even if Bregman's conditions on the criterion are compatible with a large class of functions, the algorithm is tractable only for the two expressions of F already described since Equation (10) requires a gradient inversion.

To overcome this drawback, we propose in the next section to combine Bregman's algorithm with a half-quadratic minimization approach that has been developed within the Bayesian framework.

4 Half-Quadratic Optimization

Half-quadratic optimization initially proposed by Geman and Reynolds,[13] has been extensively used in the Bayesian framework.[14] The principle consists of introducing an auxiliary variable to convert the initial nonquadratic optimization problem to a sequence of quadratic optimization problems that can be handled by standard algorithms. This approach is based on the Geman and Reynold's theorem generalized by Charbonnier *et al.*[15] by relaxing the assumption of an horizontal asymptote on the criteria.

4.1 *Geman and Reynold's Theorem*

Let us assume that $F(x)$ is an even real-valued function satisfying the following properties:

$$\lim_{x\to 0^+} \frac{F'(x)}{2x} = M < +\infty,$$

$$\lim_{x\to +\infty} \frac{F'(x)}{2x} = N \quad 0 < N < M,$$

$\frac{F'(x)}{2x}$ is a continuous and strictly decreasing function on $]0+\infty[$.

Then, a strictly convex and decreasing function Ψ defined on $[NM]$ exists such that $F(x)$ can be rewritten as:

$$F(x) = \min_{N\le b\le M} \{bx^2 + \Psi(b)\}. \tag{11}$$

Moreover, the minimum, $\min_{N\le b\le M}\{bx^2+\Psi(b)\}$, is reached for:

$$\bar{b} = \frac{F'(x)}{2x}. \tag{12}$$

In the extended version proposed by Charbonnier, $N=0$ is possible, but in the following, the derivative of the criterion F must be nonzero. Hence, we restrict the class of admissible functions to those not having a horizontal asymptote.

4.2 *Half-Quadratic Minimization*

Now, let us consider the initial problem of Equation (4) for a criterion $F(x)=\Sigma_i F(x_i)$ satisfying the preceding conditions. By abuse of notation, we identify the global vectorial criterion and the real function acting on each component of the vector $\mathbf{x}$. The reconstruction problem can be reformulated as:

$$\begin{cases} \min\limits_{x} \sum\limits_{i} \min\limits_{N\le b_i\le M} \{b_i x_i^2 + \Psi(b_i)\} \\ \text{s.t. } \mathbf{H}x = y. \end{cases} \tag{13}$$

Introducing $\mathbf{B}$ a diagonal matrix with entries b_i, and a real-valued function $\Psi(\mathbf{B})=\Sigma_i\Psi(b_i)$ the problem is written:

$$\begin{cases} \min\limits_{x} \min\limits_{\mathbf{B}} \{x^T\mathbf{B}x + \Psi(\mathbf{B})\} \\ \text{s.t. } \mathbf{H}x = y \end{cases} \tag{14}$$

The system of Equation (14) can be solved by using an alternating minimization scheme with respect to the intensity image x and the auxiliary variable $\mathbf{B}$. The minimization with respect to $\mathbf{B}$ can be performed analytically using Equation (12) and Bregman's algorithm can be used for the minimization with respect to x since the functional is quadratic in x. This leads to the following algorithm:

initialization: $x^0 = 0$.

iterative step:

minimization on $\mathbf{B}$, x being fixed to x^{n-1},

$$b^n{}_i = \frac{F'(x_i^{n-1})}{2x_i^{n-1}} \quad i=1,\ldots,m, \tag{15}$$

minimization on x, $\mathbf{B}$ being fixed to $\mathbf{B}^n$

initialization step: $x^0 = 0$

iterative equation:

$$\nabla F(x^{k+1}) = \nabla F(x^k) + H_{i_k}^T \lambda,$$

$$2\mathbf{B}^n x^{k+1} = 2\mathbf{B}^n x^k + H_{i_k}^T \lambda.$$

If S^n denotes $(\mathbf{B}^n)^{-1}$ $(0<N\le b_i\le M \forall i)$.

$$x^{k+1} = x^k + \tfrac{1}{2} S^n H_{i_k}^T \lambda,$$

with $y_{i_k} = \langle H_{i_k}, x^{k+1}\rangle$ leading to

$$\lambda = \frac{2}{H_{i_k} S H_{i_k}^T} (y_{i_k} - \langle H_{i_k}, x^k\rangle). \tag{16}$$

Hence, we have:

$$x^{k+1} = x^k + \frac{S^n H_{i_k}^T}{H_{i_k}^T S^n H_{i_k}} (y_{i_k} - \langle H_{i_k}, x^k\rangle). \tag{17}$$

Concerning the preceding algorithm note that

- Since $x^0=0$, b^0 is uniform and the first iteration is equivalent to an estimation using the standard ART algorithm.
- After each estimation of the variable $\mathbf{B}^n$, the current estimate x should be reset to zero to satisfy Bregman's initial conditions.

- The variable $s^n = 1/b^n$ acts as an indicator of the support of the object. This can be shown by taking the augmented objective function $F^*(x,S) = \Sigma_i 1/s_i x_i^2 + \Psi(1/s_i)$. When s_i has a low value, x_i should be near 0 to minimize F^*, whereas the higher s_i, the more free x_i is.
- The support S^n computed after each convergence of the Bregman's algorithm is related to the density by $s(x_i) = 1/b_i = 2x_i/F'(x_i)$. This function does not need to be normalized since it is implicitely done in Equation (17).
- Here $S\,\mathbf{H}_i^T$ defines a nonuniform backprojection or a backprojection on a "fuzzy" support defined by the membership function $s(x) = 2x/F'(x)$. This operator satisfies the conditions stated by Herman[16] to define a backprojection operator, i.e.:
  - A ray should contribute to those pixels which it intersects and not to others.
  - The contribution of the i'th ray to a pixel should be proportional to y_i (the measured data for the i'th ray).
  - The contribution of the i'th ray to the j'th voxel should be proportional to h_{ij}.

The half-quadratic algorithm alternates successively a support-driven reconstruction and an estimation of the support using the prior densitometric information. This scheme overcomes limitations of Gerchberg-Papoulis algorithm. First the unknown support is progressively estimated during the reconstruction process using densitometric prior information by the intermediate of the support function. Second, the use of a nonbinary support enables us to have a wide support whose Fourier transform may differ from a Dirac kernel and is wide enough to provide a significant extrapolation.

4.3 *Convergence Analysis*

4.3.1 *Convergence of the global criterion*

Let us note that $J(\mathbf{B},x) = x^T\mathbf{B}x + \Psi(\mathbf{B}) = \Sigma_i b_i x_i^2 + \Psi(b_i)$,

$$J_n = J(\mathbf{B}^n, x^n).$$

The minimization on $\mathbf{B}$ at step n leads to:

$$J(\mathbf{B}^{n-1}, x^{n-1}) \leq J(\mathbf{B}, x^{n-1}) \forall \mathbf{B}.$$

Since x_n results from the minimization of $J(\mathbf{B}^n, x)$ on $\mathbf{x}$, we have:

$$J(\mathbf{B}^n, x^n) \leq J(\mathbf{B}^n, x) \forall x \text{ such that } \mathbf{H}x = y.$$

Thus

$$\begin{aligned} J_{n-1} - J_n &= J(\mathbf{B}^{n-1}, x^{n-1}) - J(\mathbf{B}^n, x^n) \\ &= \underbrace{J(\mathbf{B}^{n-1}, x^{n-1}) - J(\mathbf{B}^n, x^{n-1})}_{\geq 0} \\ &\quad + \underbrace{J(\mathbf{B}^n, x^{n-1}) - J(\mathbf{B}^n, x^n)}_{\geq 0}. \end{aligned}$$

Moreover because J_n is positive, we have $J_{n-1} \leq J_n \leq 0$, which ensures the convergence of J_n.

4.3.2 *Convergence of the auxiliary variable*

Let us now consider the real function $g(b) = b(x^n)^2 + \Psi(b)$ where b stands for any component of the diagonal matrix $\mathbf{B}$. Using Taylor's theorem, we can write:

$$\begin{aligned} g(b^{n-1}) &= g(b^n) + (b^{n-1} - b^n) g'(b^n) \\ &\quad + \tfrac{1}{2} (b^{n-1} - b^n)^2 g''(\alpha) \end{aligned}$$

with $\alpha \in [b^{n-1}, b^n]$. Considering now that b^n results from the minimization of g, we have $g'(b^n) = 0$. Then:

$$g(b^{n-1}) - g(b^n) = \tfrac{1}{2}(b^{n-1} - b^n)^2 g''(\alpha).$$

Moreover, $g'' = \Psi''$ and it exists $c > 0$ such that $\Psi'' \geq c$ (consequence of the strict convexity of Ψ). Thus

$$0 \leq \frac{c}{2} (b_{n-1} - b_n)^2 \leq g(b_{n-1}) - g(b_n),$$

and since:

$$g(b_{n-1}) - g(b_n) = J(b^{n-1}, x^n) - J(b^n, x^n) \leq J_{n-1} - J_n,$$

we have:

$$0 \leq \frac{c}{2} (b^{n-1} - b^n)^2 \leq J_{n-1} - J_n,$$

which shows the convergence of (b^n).

4.3.3 *Convergence of the algorithm*

Let us first remark that $\|x^n\|$ remains bounded since:

$$+\infty > J_0 \geq J_n \geq \sum_i b_i^n (x_i^n)^2 + \Psi(b_i^n) \geq N \|x^n\|^2.$$

Consider now the pair $(\mathbf{B}^n, x^n)$ obtained after the minimization in x. Using Lagrange optimality Equation (6), it exists λ^n such that: $\nabla F(x^n) = \mathbf{B}^n x^n = -\mathbf{H}^T \lambda^n$. Hence, $\mathbf{B}^n x^n$ belongs to the range space of $\mathbf{H}$ and considering that x^n and x^{n+1} differ only by their null-space component, we have:

$$\langle \mathbf{B}^n x^n - \mathbf{B}^{n+1} x^{n+1}, x^n - x^{n+1} \rangle = 0.$$

Introducing $\mathbf{B}^{n+1} x^n$ leads to:

Table 1 Criteria and their associated support functions commonly used within the Bayesian regularizing framework.

	Criterion Expression	Support Function
Convex functions	$f_1 \equiv x^2$	$s_1 \equiv 1$
	$f_2 \equiv \lvert x \rvert^{\alpha} 1 \leq \alpha < 2$	$s_2 \equiv \frac{2\lvert x \rvert^{2-\alpha}}{\alpha}$
	$f_3 \equiv \log[\cosh(x)]$	$s_3 \equiv \frac{x}{\tanh(x)}$
	$f_4 \equiv 2(\sqrt{1+x^2}-1)$	$s_4 \equiv (1+x^2)^{1/2}$
Nonconvex functions	$f_5 \equiv \log(1+x^2)$	$s_5 \equiv 1+x^2$
	$f_6 \equiv 1-\exp(-x^2)$	$s_6 \equiv \exp(x^2)$
	$f_7 \equiv \frac{x^2}{1+x^2}$	$s_7 \equiv (1+x^2)^2$

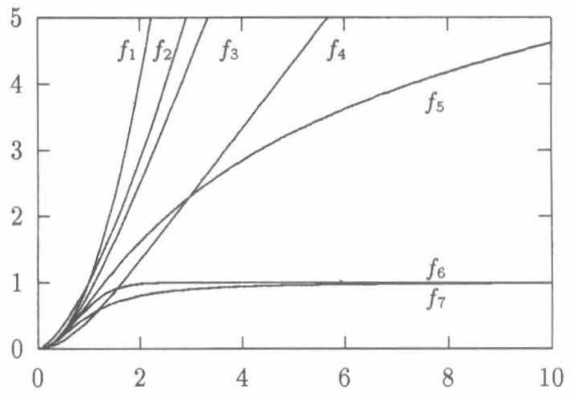

Fig. 3 Behavior of the criteria.

$$\langle (\mathbf{B}^n - \mathbf{B}^{n+1})x^n, x^n - x^{n+1} \rangle + \langle \mathbf{B}^{n+1}(x^n - x^{n+1}), x^n - x^{n+1} \rangle = 0.$$

Since $\|x^n\|$ is bounded and $\mathbf{B}^{n+1}$ is minored, it exists α and β real numbers which are strictly positive, such that:

$$0 \leq \beta \|x^n - x^{n+1}\| \leq \alpha \|\mathbf{B}^n - \mathbf{B}^{n+1}\| .$$

Then, the global convergence of the algorithm results from the convergence of $\mathbf{B}^n$.

In conclusion, if F is a convex function, the algorithm converges to the unique solution of Equation (4). If F is a nonconvex (but agrees with the conditions stated by the Geman and Reynolds theorem), it is convergent to a stationary point (eventually a local minima) of the initial problem. This condition can be summarized by "if the support function is increasing and bounded, the global convergence is guaranteed." We should observe that Geman and Reynolds' conditions imply that the support function is never zero, but this condition can be relaxed if we specify that when $s_i = 1/b_i$ is zero, the associated voxel x_i remains 0 for all further iterations. Then, the estimate x^n and the criterion remain bounded and all the proof already developed stands. The only constraint is then to initialize the support at the first iteration to a nonzero uniform value. For very small s_i, we should note the convergence of the algorithm is not affected since s appears both in the numerator and the denominator of Equation (17).

4.4 *Examples of Criteria*

The key of the optimization problem relies on the choice of the criteria F, which determines how the intensity of each voxel is penalized. For instance, choosing the classic quadratic criterion $F(x) = x^2$ will cause high intensity to be heavily penalized and therefore will result in low contrast images. The corresponding support function does not depend on x and the algorithm tends to spread the density over every voxel. By choosing a function F whose behavior is linear, high intensity values will be less penalized and the corresponding support function is proportional to the estimated density. A horizontal behavior of the criteria will favor high values and will tend to hyperconcentrate the density.

A brief review of the criteria proposed within the Bayesian regularization framework is given in Table 1 and in Figs. 3 and 4. The criteria f_5, f_6, and f_7 do not exactly fulfill the conditions required since their associated support functions are not bounded. To overcome this drawback, an extra quadratic constraint αx^2 can be added to the initial criterion to introduce a saturation in the support function, which is then defined by:

$$s(x) = \frac{1}{[F'(x)/2x] + \alpha}. \tag{18}$$

If the weighting factor α is chosen small enough, the support function still behaves like the one given in Table 1 for the range of density used. Nevertheless, when the support function increase too rapidly—such as for s_5 to s_7—the reconstruction appears to be very unstable and the precision of the convergence for the minimization in x seems to be very sensitive and the weighting factor α should not be negligible. For instance, function $f_7 = x^2/(1+x^2)$ is stabilized by adding αx^2. The associated support function is proportional to:

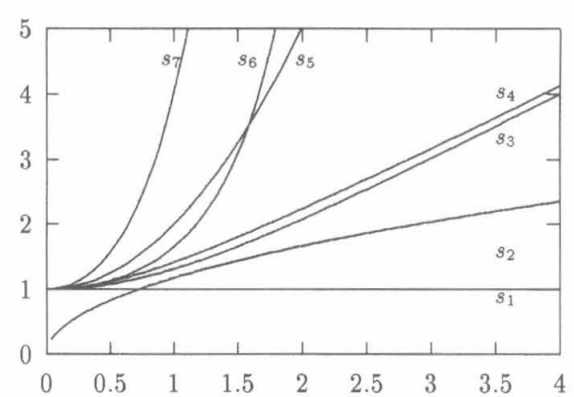

Fig. 4 Behavior of the support functions.

$$1-\frac{1}{1+\alpha(1+x^2)^2}$$

4.5 *Taking Noise into Account*

To take into account the data errors (noise, roundoff error, etc.), the observation equation is often relaxed as follows:

$$\mathbf{H}x = y + \epsilon, \tag{19}$$

where ϵ represents the error vector. A regularizing procedure requires further prior knowledge about the noise.

Assuming that the noise follows a Gaussian distribution, a quadratic constraint on the noise ϵ can be incorporated into the noiseless criterion to form the following problem:

$$\begin{cases} \min\limits_{x,\epsilon} F(x) + \dfrac{1}{\alpha}\|\epsilon\|^2 \\ \text{s.t. } \mathbf{H}x - I\epsilon = y \end{cases}, \tag{20}$$

where α acts as the standard deviation of the noise. Using the extended variables $z^T = [x_1, \ldots, x_n, \epsilon_1, \ldots, \epsilon_m]^T$ and the matrix $[\mathbf{H}|-I]$ defined by:

$$\begin{bmatrix} h_{11} & .. & .. & h_{1n} & -1 & 0 & .. & .. & 0 \\ .. & .. & .. & .. & 0 & -1 & .. & .. & 0 \\ .. & .. & .. & .. & 0 & .. & .. & -1 & 0 \\ h_{m1} & .. & .. & h_{mn} & 0 & .. & .. & 0 & -1 \end{bmatrix},$$

the previously developed approach can be applied and the internal minimization on x using Bregman algorithm leads to the following iterative scheme:

initialization step: $\begin{cases} x^0 = 0 \\ \epsilon^0 = 0 \end{cases}$,

iterative equation: $\begin{cases} x^{k+1} = x^k + \frac{1}{2} S H_i^T \lambda_k \\ \epsilon^{k+1} = \epsilon^k - \alpha I_i^T \lambda_k \end{cases}$,

with: $\lambda_k = \dfrac{1}{\alpha + H_{i_k} S H_{i_k}^T}(y_{i_k} - H_{i_k} x^k + I_{i_k} \epsilon^k)$.

This section shows the link with Bayesian regularization and provides an approach for applying more complex noise model by the use of nonquadratic criteria on ϵ. Note that taking noise into account is of a great importance since spectrum extrapolation implies the restoration of high frequency components, i.e., very unstable components.

5 Results

In this section, the developed algorithm is applied to simulated and real data, and the results are compared. We are mainly interested in the 3D vascular imaging in which the limited number of projections leads to a densitometric underestimation of small blood vessels and undersampling artifacts. The first section deals with different expressions of the criterion compared to standard algorithms such as ART or MART on simulated data. In the second section, experimental results on clinical data are shown and discussed.

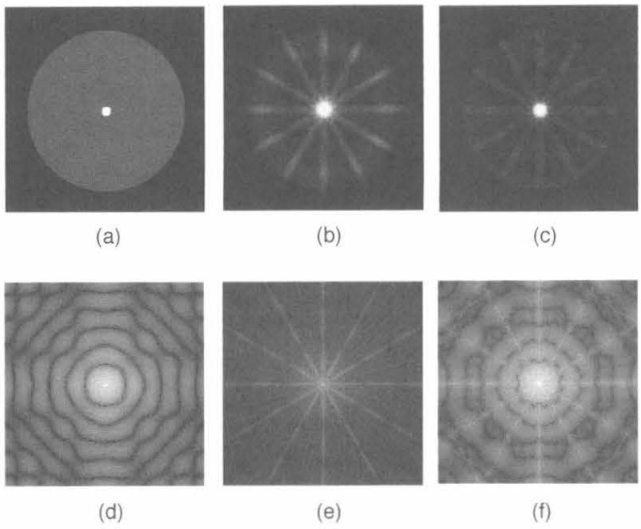

Fig. 5 (a) Original object, (b), ART reconstruction, (c) MART reconstruction, and (d), (e) and (f) respective Fourier transforms of (a), (b) and (c).

5.1 *Simulated Data*

To represent a typical highly contrasted vessel surrounded with a low density background, we simulated a 3D image of a cylinder (density 100) of diameter 6 voxels with a background designed by an other cylinder of density 5 and diameter 200 voxels. For this simulation, six projections equally distributed over 180 deg were used.

Figure 5(a) shows a 2D axial cross section of the original object and Figs. 5(b) and 5(c) the reconstructions obtained using ART and MART algorithms. In Figs. 5(d), 5(e), and 5(f), the 2D Fourier transform of images of Figs. 5(a), 5(b) and 5(c) are displayed.

Using ART [Fig. 5(b)], the central spot is spread over six line-artifacts corresponding to the six projection directions. This results in a densitometric underestimation of the central spot. Figure 5(e), displaying the Fourier transform of the ART reconstruction, illustrates the projection theorem (see Section 2) and demonstrates that linear methods are unable to handle null-space components.

Using MART [Fig. 5(c)], the cylinder is better recovered with less dense undersampling artifacts. This is due to the nonlinearity of MART, which enables extrapolation of the missing sectors in the Fourier space. Nevertheless, some artifacts remain. To remove them, we propose to use the constrained optimization approach already developed. The problem that arises now is how to choose the criterion.

We tested various criterion expressions; the first one corresponds to function f_4 of Table 1, the second to function f_7 and for the third a quadratic stabilizing term $0.1x^2$ has been added to f_7. Moreover, each of these functions have been rescaled by normalizing x by 30. The criteria f_4 and f_7 have been chosen since they exhibit typical behavior. The criteria f_2 and f_3 lead to results similar to those obtained with f_4, whereas f_5 and f_6 present an horizontal asymptot like f_7.

The first criterion expression, f_4 [Figs. 6(a) and 6(b)] exhibits an asymptotic behavior similar to that in the case of the entropic constraint. The reconstructed object as well

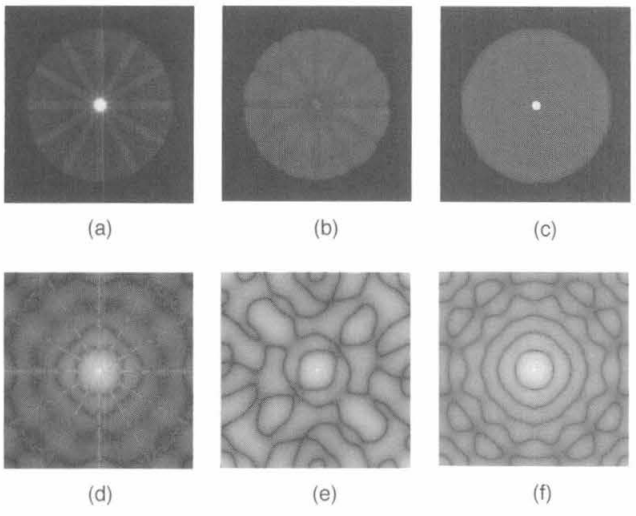

Fig. 6 Reconstruction using (a) f_4, (b) f_7, and (c) $f_7+0.1x^2$; (d), (e) and (f) respective Fourier transforms of (a), (b) and (c).

as the Fourier transform are very similar to those reconstructed by MART.

The second criterion presenting a horizontal asymptote no longer penalizes high intensity objects (i.e., intensity in the range of the plate of the criterion). This gives rise to very unstable reconstructions with overshots and oscillations [Fig. 6(b)]. The density is so concentrated that "negative" artifacts (compared to the mean level) appear in the background.

To overcome this instability, the third criterion was built by adding a "stabilizing" quadratic term to the previous one. The recovered object [Fig. 6(c)] is very similar to the original one with only small oscillations of the density. Its Fourier transform [Fig. 6(f)] is quite close to the original one [Fig. 5(d)] compared to the others.

To test the algorithm with a limited-angle acquisition, we apply it for the reconstruction of a large cylinder whose projection set is composed of six projections equally spaced on 90 deg. The results are displayed in Fig. 7. Compared to the original object [Fig. 7(a)], the ART reconstruction [Fig. 7(b)] shows the limitations of linear methods, which are also clearly revealed in the Fourier domain [Fig. 7(g)]. The simple use of a positivity constraint [Figs. 7(c) and 7(h)] enable us to suppress the negative artifacts, which results in the restoration of a far better cylinder. But the deformation of the object remains. This is well illustrated in the Fourier domain [Fig. 7(h)], where the positivity constraint provides an extrapolation only in the neighborhood of the known data and cannot lead to a significant extrapolation onto the missing sectors. Note also that the positivity constraint is useless when a nonzero background exists, such as in the previous simulation.

Using MART [Fig. 7(d)], the original object is much better recovered and Fig. 7(i) demonstrates the spectrum extrapolation performed using the maximum entropy criterion. Some wave-shaped artifacts appear in the recovered missing sector.

Using the same criteria as for Fig. 6(c), a better isotropic recovery of the object with sharper edges is performed. The analysis of the Fourier transform [Fig. 7(j)] shows the isotropy of the reconstruction with the two recovered sectors being a little less dense than the known sectors. Nevertheless, this demonstrates the power of the use of the developed algorithm with criteria including densitometric priors for the recoverage of simple shape object.

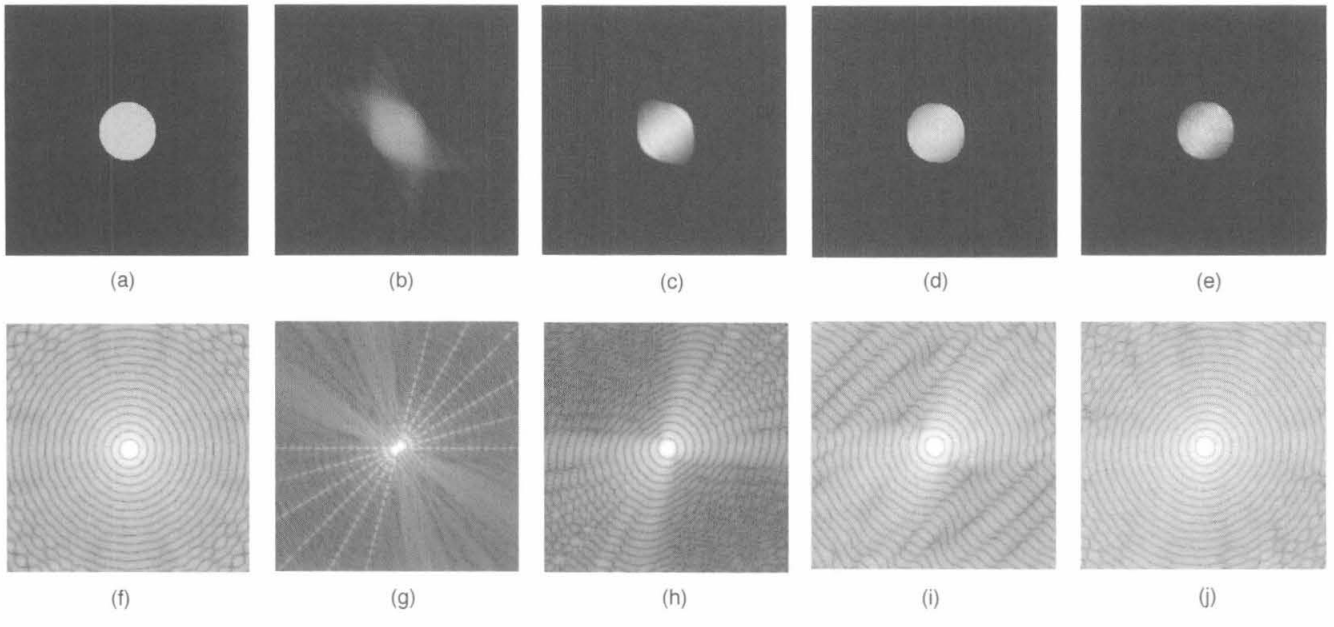

Fig. 7 (a) Original object, (b) ART reconstruction of (a), (c) ART reconstruction of (a) with a positivity constraint, (d) MART reconstruction of (a), (e) reconstruction using the same criteria as for Fig. 6(c), (f), (g), (h), (i), and (j), the respective Fourier transforms of (a), (b), (c), (d), and (e).

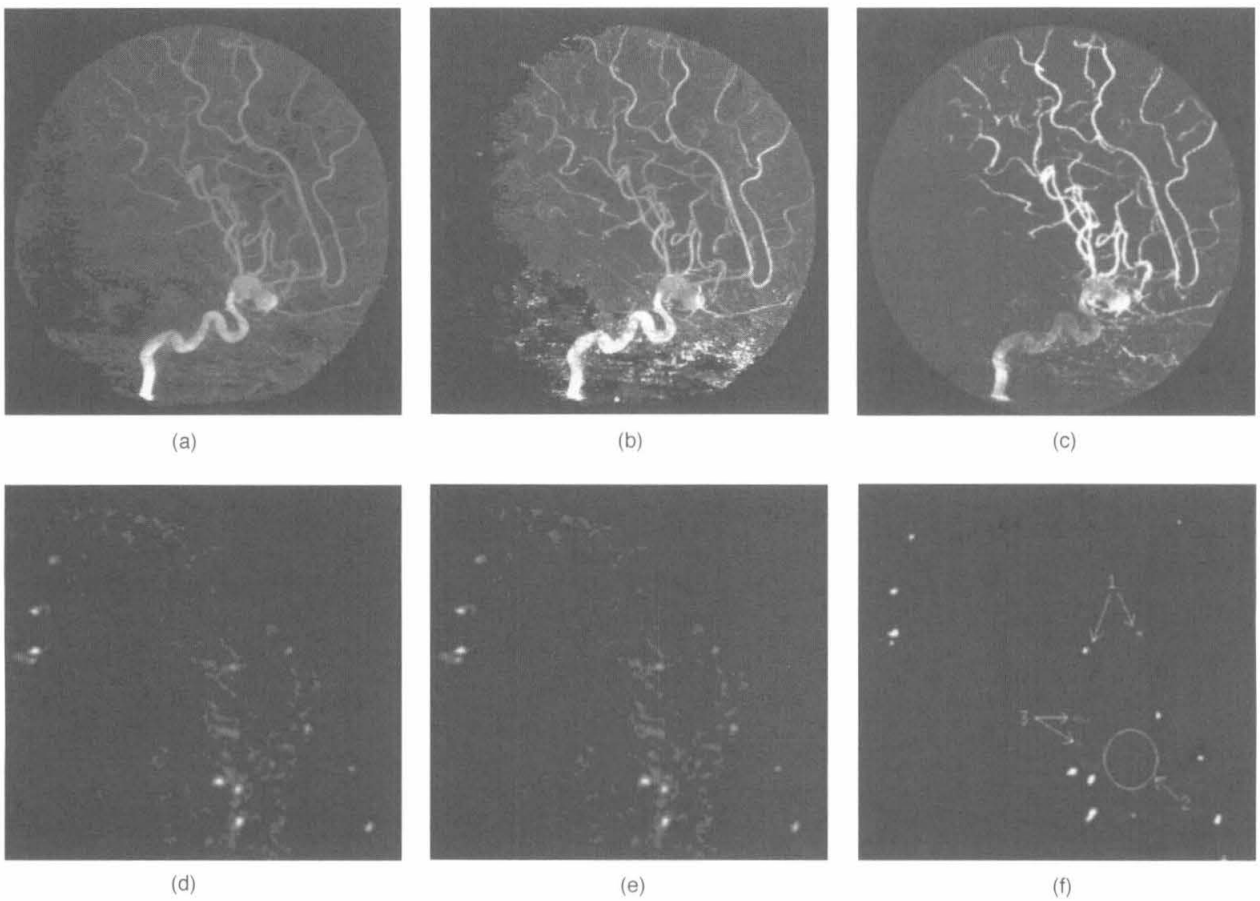

Fig. 8 (a) ART reconstruction, (b) MART reconstruction, (c) reconstruction using criterion $f_7+0.1x^2$. (d), (e) and (f). Detail of an axial cross-section of, respectively (a), (b) and (c).

5.2 *Application to Clinical Vascular Data*

In the previous section, various criteria adapted to the reconstruction of small objects with high density were introduced and their influence on the reconstruction were investigated and compared to standard algorithms. The same approaches were applied to clinical vascular data. The data set consists of 18 2D-DSA equally distributed over 180 deg and the reconstructed images have a size of 256^3. Results obtained using ART, MART and the constrained optimization approach (with the criterion $f_7+0.1x^2$) are respectively displayed in Fig. 8. These results raise the following comments:

1. The small vessels are enhanced using nonquadratic criteria [compare Fig. 8(a) to Figs. 8(b) and 8(c)]. The constrained optimization with criterion $f_7 0.1x^2$ tends to concentrate the density on the vessels; this appears either through the increase of the vessel density or through the decrease of the background mean level. The enhancing effect can also be observed on the axial cross-section view; see, for instance, the small vessels labeled 1 in Fig. 8(f).
2. The undersampling artifacts are reduced using the proposed algorithm. This appears clearly in the cross-section; looking at the area labeled 2 in Fig. 8(f); the background is more homogenous than on Figs. 8(d) and 8(e).
3. Nonquadratic criteria that tend to concentrate the density to enhance the contrast of small vessels are much more noise sensitive. This appears Figs. 8(b) and 8(c), which present noisy structures in the bottom right. Using ART [Fig. 8(a)], the data errors are spread uniformly over each ray, whereas the errors are concentrated in a few voxels by the other algorithms. The small spot labeled 3 in Fig. 8(f) corresponds to such concentrated noise.

This effect of density concentration is enhanced by the quadratic behavior of the support function in the range of the values corresponding to the background density. Hence, to suppress this effect we built an *ad hoc* support function whose analytical form is given in Appendix A and its behavior is shown in Fig. 9 for 2 couples of parameters. Note that the criterion corresponding to this support function cannot be analytically expressed. This function is composed of a first uniform part ($x \leq k_{\min}$), whose density range correspond to the background (parenchyma) level. Then, after a quadratic transition part, the support function in-

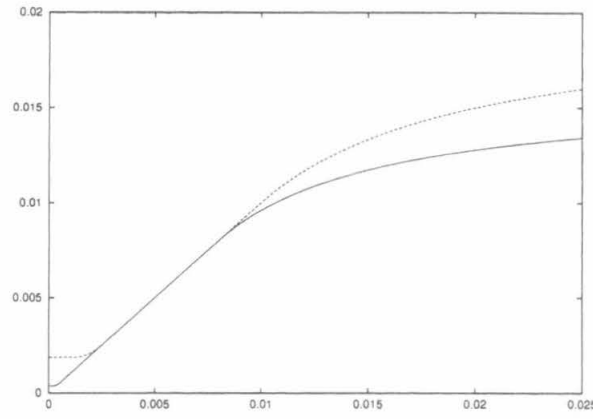

Fig. 9 Support function for 2 couples of parameter (k_{min},k_{max}): (0.0002, 0.008) and (0.001, 0.01).

creases in a linear way up to a value k_{max} from which the function begin to slowly saturate. The density range of this linear portion is chosen to correspond to the density of the small vessels, which are usually underestimated, and the k_{max} value is fixed to the nominal attenuation value of a opacified vessel. The progressive saturation is performed to ensure the convergence of the algorithm.

Figure 10 compares the results obtained using this function to those obtained with ART on a 512^3 reconstruction from 36 projection equally spaced on 180 degrees. The maximum intensity projections (MIP) as well as the cross-sections are displayed within the same dynamic range. First, we note the enhancement of the density of the vessel using the *ad hoc* function. This is clearly visible around the aneurysm in the central part of Figs. 10(a) and 10(b). We also notice the lower background value in Fig. 10(d). On the cross-sections [Figs. 10(b), 10(c), 10(e), and 10(f)], the small vessels appear far better contrasted and the background is wider with a lower and more uniform value. Compared to the results obtained with criteria $f_7+0.1x^2$, we notice that the noisy aspect has disappeared by imposing a flat behavior to the support function in the density range of the background.

In Fig. 11, results obtained with a limited-angle acquisition are displayed. The data set consists of 18 projections distributed on 120 deg. The MIP views [Figs. 11(a) and 11(b)] correspond to a projection angle that does not belong to the acquisition sector.

In the MIP views, the contrast enhancing effect and the better definition of the vascular structure obtained using the support function is clearly visible. Compare, for instance, the small vessels in the top right of the MIP views which are very blurred with the ART algorithm.

In cross-sections [Figs. 11(b) and 11(d)], we observe the same effect, and the deformation of the aneurysm (the big white spot in the bottom center) is reduced, but it still remains. The relative weakness of reduction of the deformation compared to that obtained in simulation may be due to the design of the support function. On simulation, the sup-

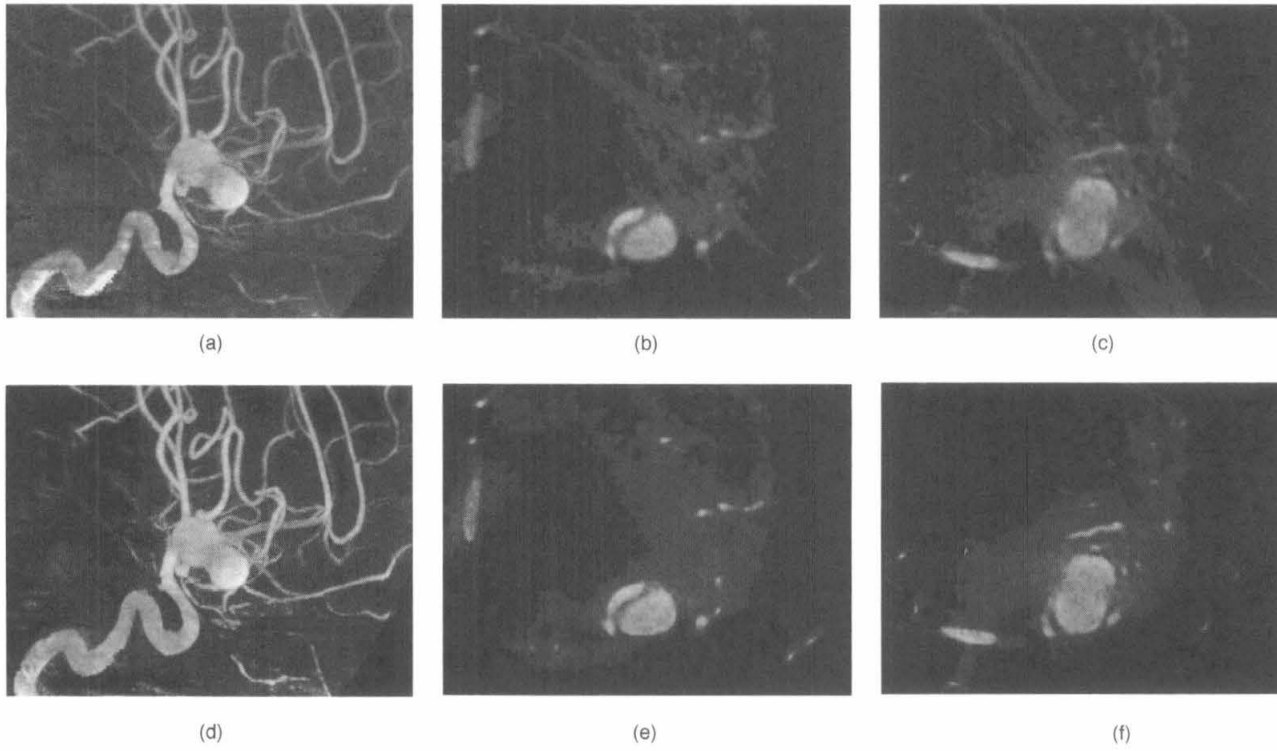

Fig. 10 Reconstruction from a data set composed of 36 projections equally spaced on 180 deg. First row: ART reconstruction (a) MIP view, (b) and (c) horizontal cross-sections through the aneurysm. Second row: reconstruction using the support function previously defined (k_{min}=0.001, k_{max}=0.01) (d) MIP view, (e) and (f) horizontal cross-sections through the aneurysm.

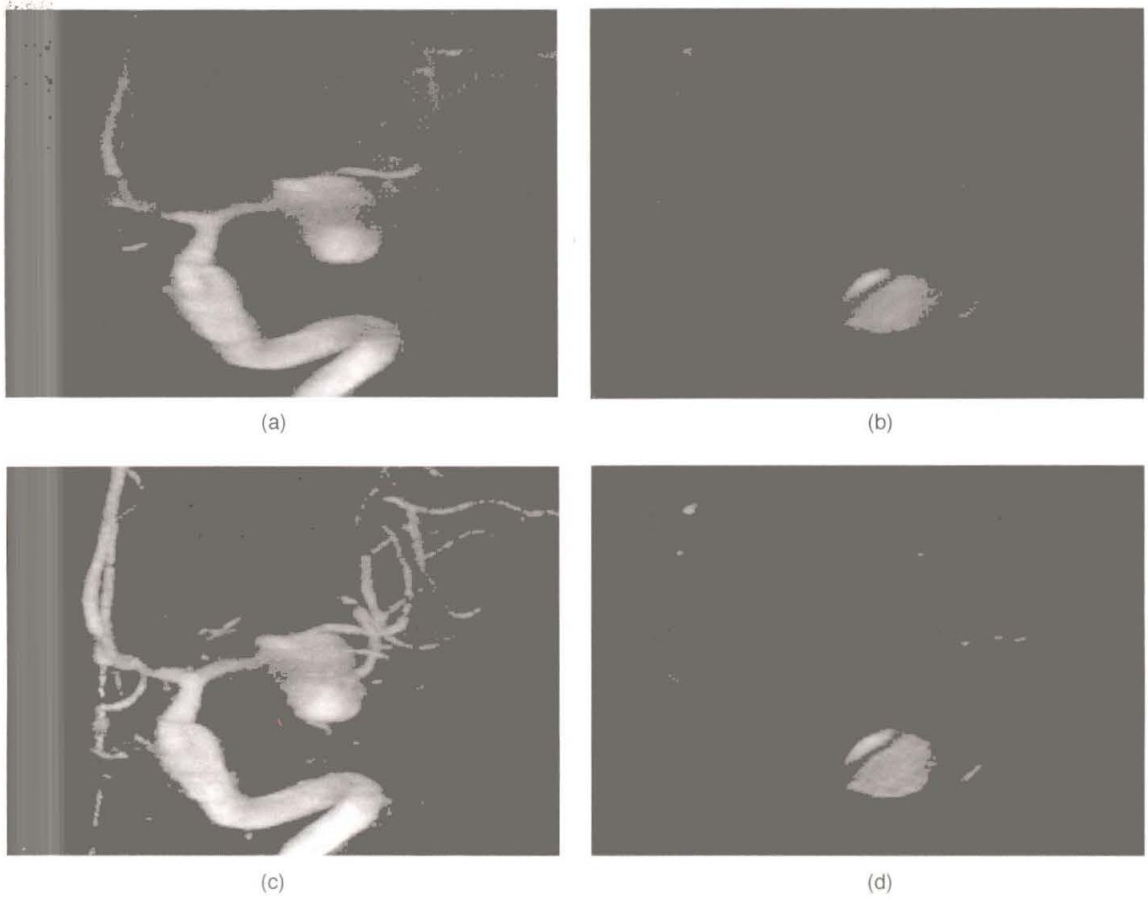

Fig. 11 Recontruction from a data set composed of 18 projections distributed on 120 deg. First row: ART reconstruction (a) MIP view and (b) horizontal cross-section through the aneurysm. Second row: reconstruction using the support function previously defined ($k_{min}=0.001$, $k_{max}=0.01$) (c) MIP view and (d) horizontal cross-section through the aneurysm.

port function used increases locally in a quadratic way and can hyperconcentrate density, whereas the *ad hoc* function, which increases only in a linear way, seems to have lost this property.

6 Conclusions

In this paper, the problem of 3D reconstruction from an incomplete data set has been addressed. Within the constrained optimization framework, a nonzero null-space component of the null space of the acquisition matrix can be reconstructed by the minimization of a given criterion. A deterministic relaxation algorithm based on Bregman's algorithm combined with half-quadratic minimization techniques has been proposed for the minimization of a large class of criteria.

Simulation of numerical data has shown the value of such an approach for the extrapolation of the missing sectors in the Fourier domain. Application to vascular data demonstrates the effectiveness of the proposed approach for enhancing small vessels and reducing the deformation due to limited angular data.

7 Appendix A

The analytical form of the *ad hoc* support function is

$$s(x)=\begin{cases} 3\dfrac{k_{\min}}{2} & \text{if} \quad x\leq k_{\min} \\ \dfrac{1}{2}\dfrac{x^2}{k_{\min}}-x+2k_{\min} & \text{if} \quad k_{\min}\leq x\leq 2k_{\min} \\ x & \text{if} \quad 2k_{\min}\leq x\leq k_{\max} \\ k_{\max}\left(2-\dfrac{k_{\max}}{x}\right) & \text{if} \quad k_{\max}\leq x. \end{cases}$$

References

1. H. K. Tuy, "An inversion formula for cone-beam reconstruction," *SIAM J. Appl. Math.* **43**, 546–552 (1983).
2. A. Klug and R. A. Crowther, "Three dimensional image reconstruction from the view point of information theory," *Nature* **228**, 435–440 (1972).
3. R. W. Gerchberg, "Super-resolution through error energy reduction," *Opt. Acta* **21**, 709–720 (1974).
4. A. Papoulis, "A new algorithm in spectral analysis and band-limited extrapolation," *IEEE Trans. Circ. Syst.* **CAS-22**, 735 (Sep. 1975).
5. T. S. Sato, M. Linzer, S. J. Norton, O. Ikeda, and M. Hirama, "Tomographic image reconstruction from limited projections using itera-

tive revisions in image and transforms space," *Appl. Opt.* **20**(3), 395–399 (1981).
6. M. Defrise and C. de Mol, "A regularized iterative algorithm for limited-angle inverse radon transform," *Opt. Acta* **30**(4), 403–408 (1983).
7. E. T. Jaynes, "Information theory and statistical mechanics I and II," *Phys. Rev.* **106**, 629–630; **108**, 171–190 (1957).
8. G. T. Herman, R. Gordon, and R. Bender, "Algebraic reconstruction technic (ART) for three dimensional electron microscopy and x-ray photography," *J. Theor. Biol.* **29**, 471–481 (1970).
9. A. Lent, "A convergent algorithm for maximum entropy image restoration, with a medical x-ray application," in *Proc. SPSE Conf.*, pp. 249–257 (1977).
10. G. Minerbo, "MENT: a maximum entropy algorithm for reconstructing a source from projection data," *Comput. Graph. Image Process.* **10**, 48–68 (1979).
11. N. J. Dusaussoy and I. E. Abdou, "The extended MENT algorithm: a maximum entropy-type algorithm using prior knowledge for computerized tomography," *IEEE Trans. Signal Process.* **39**(5), 1164–1180 (1991).
12. L. M. Bregman, "The relaxation method of finding the common point of convex sets and its application to the solution of problems in convex programming," *USSR Comput. Math. Mathemat. Phys.* **7**, 200–217 (1967).
13. D. Geman and G. Reynolds, "Constrained restoration and the recovery of discontinuities," *IEEE Trans. Pattern Anal. Intell.* **14**(3), 367–383 (1992).
14. P. Charbonnier, "Reconstruction d'image: régularisation avec prise en compte des discontinuités," PhD thesis, Université de Nice-Sophia Antipolis (1994).
15. P. Charbonnier, M. Barlaud, L. Blanc-Feraud, and G. Aubert, "Deterministic edge-preserving regularization in computer imaging," *IEEE Trans. Image Proc.* (Jan. 1997).
16. G. T. Herman, *Image Reconstruction from Projections, the Fundamental of Computerized Tomography*, Academic Press (1980).

Etienne Payot received an engineering degree in 1990 from the Institut de Chimie et de Physique Industrielles, Lyon, France, and a PhD degree in 1996 from the Ecole Nationale Supérieure des Télécommunications, Paris, France. His main interests include 3D imaging and image processing.

Françoise J. Prêteux is currently a professor and heads the Department of Signal and Image Processing at the Institut National des Télécommunications (INT), Evry, France. Her research activities are in pattern recognition, image analysis and more specifically stochastic modeling, mathematical morphology and scene deformation analysis. She is a member of the editorial board of the Journal of Electronic Imaging and is cochair of the Statistical and Stochastic Methods for Image Processing Conference (SPIE). She also serves as a member of numerous conference committees associated with professional organizations in this field. Prêteux graduated from the Ecole des Mines de Paris in 1982 and received her Thèse d'Etat in mathematics from the University de Paris VI in 1987. Before joining INT, she was a research engineer at the Mathematical Morphology Center of Fontainebleau and was a consultant for several industrial companies from 1982 to 1989. She was then a professor in the Image Processing Department, at the Ecole Nationale Supérieure des Télécommunications from 1989 to 1993.

Yves Trousset received an engineering degree in 1983 from the Ecole Nationale Supérieure des Télécommunications (ENST), Paris, France, and the PhD degree in 1987 from ENST. He is currently a research engineer with General Electric Medical Systems, Buc, France. His main interests include image and volume reconstruction from projections, parallel processing and medical image processing.

Régis Guillemaud is an engineer and graduated from the Institut National Polytechnique de Grenoble in 1985. He has been involved in vision systems for geophysics and for autonomous robot, and in 3D single photon emission computed tomography (SPECT) imaging projects. His main interests are image processing and 3D medical imaging.